Single-plane versus three-plane methods for relative range error evaluation of medium-range 3D imaging systems
MacKinnon, David K.; Cournoyer, Luc; Beraldin, J.-Angelo

National Research Council Canada   Conseil national de recherches Canada

Canada

Single-plane versus Three-plane Methods for Relative Range Error Evaluation of Medium-range 3D Imaging Systems

David K. MacKinnon*, Luc Cournoyer, J.-Angelo Beraldin

National Research Council Canada, 1200 Montreal Road, Ottawa, Ontario, Canada

ABSTRACT

Within the context of the ASTM E57 working group WK12373, we compare the two methods that had been initially proposed for calculating the relative range error of medium-range (2 m to 150 m) optical non-contact 3D imaging systems: the first is based on a single plane (single-plane assembly) and the second on an assembly of three mutually non-orthogonal planes (three-plane assembly). Both methods are evaluated for their utility in generating a metric to quantify the relative range error of medium-range optical non-contact 3D imaging systems. We conclude that the three-plane assembly is comparable to the single-plane assembly with regard to quantification of relative range error while eliminating the requirement to isolate the edges of the target plate face.

Keywords: relative range error, 3D imaging system, lidar, performance assessment, medium-range optical non-contact 3D imaging system, terrestrial laser scanners, ASTM E57 standards development

1. INTRODUCTION

The proposed ASTM E57.02 standard "New Practice for Evaluation of Relative Range Error for Medium-Range 3D Imaging Systems" being developed by the ASTM working group WK12373 describes a method for determining the relative range error (R_{error}) of medium-range laser scanners. This method involves calculating the distance between the geometric centers of two best-fit planes (single-plane method); however, this method assumes that the edges of the planes can be isolated with reasonable accuracy. We propose an alternative method: calculate the distance between the derived points-of-intersection (POIs) of three non-parallel planes (three-plane method). Specifically, the derived POI of an arrangement of three mutually non-parallel planes, each oriented at approximately 30 degrees to the line-of-sight (LOS) of the medium range instrument under test (IUT), is obtained at two positions along the LOS. The relative range distance becomes the distance between the derived POIs at each of the two positions, and the relative range error becomes the difference between the relative range distance calculated using the IUT and relative range distance calculated using the reference instrument (RI).

In this paper we compare the relative range error and observed fit residual uncertainty of the single-plane and three-plane relative range error assessment methods. We also identify potential issues that may arise in future attempts to make relative range error assessments traceable in cases where the scanning environment, surface material and scanning geometry are tightly controlled. From this assessment, we compare the three-plane and single-plane methods, highlighting the strengths and weaknesses of each method. In Section 2 we provide background information regarding optical non-contact 3D imaging systems operating in the medium range, as well as a survey of contemporary literature regarding factors that could potentially affect range measurement error. In Section 3 we describe the single-plane and three-plane methods and in Section 4 we compare the ability of the single-plane and three-plane methods to generate relative range error values. We conclude that both methods are comparable with regard to generated relative range error values but the three-plane POI method avoids the problem of identifying target plate face edges in measurement results.

2. BACKGROUND

Range measurement error can be used to assess the performance of optical non-contact 3D imaging systems operating in the medium range. A series of range measurement error assessments performed within a short period of time and under near-identical conditions can be used to generate bias[33] and uncertainty[33] values from the mean and standard deviations of the error measurements respectively. In order to better understand the factors affecting range measurement error it is useful to first detail those factors that are known to affect range measurement uncertainty.

*david.mackinnon@nrc-cnrc.gc.ca; phone 1 613 993-0114; fax 1 613 952-0215

In this section we summarize the technological bases for common medium range systems before describing the various factors affecting range measurement uncertainty with special focus on external factors, which can't easily be quantified by the manufacturer of the system so must be assessed by the system operator.
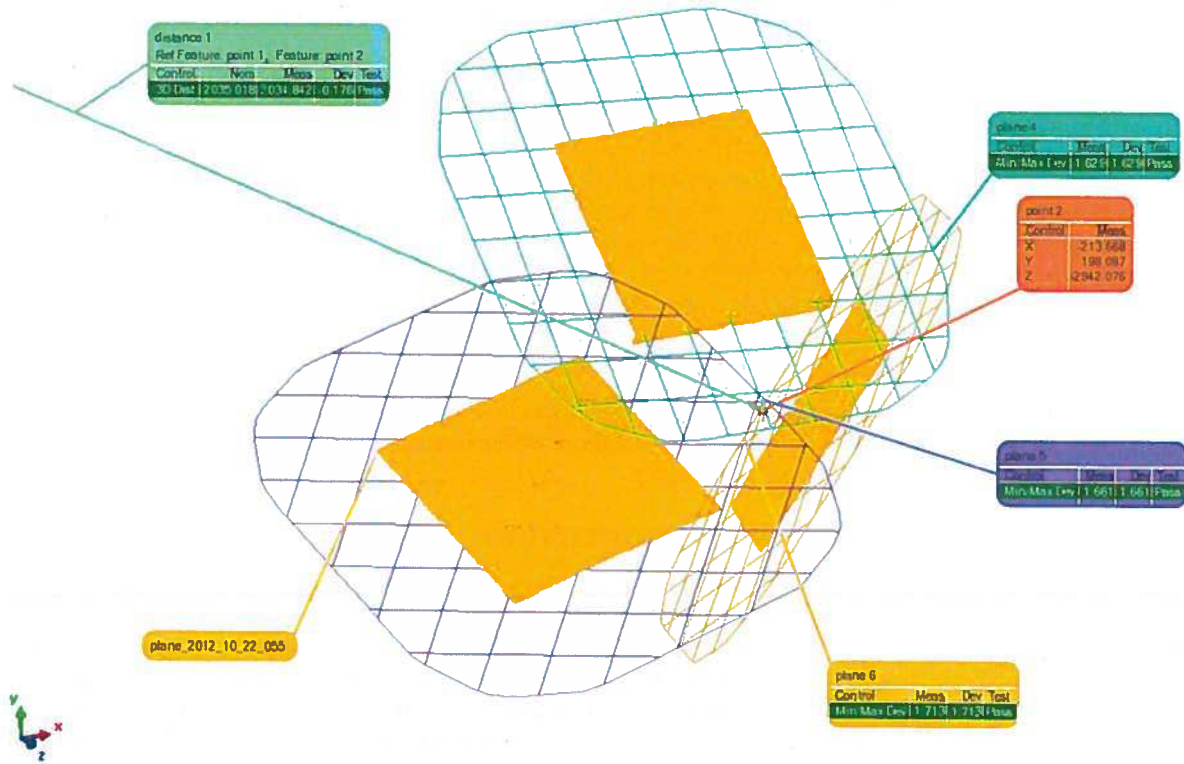

Figure 1. Three-plane assembly with derived point of intersection (POIs) labeled as "point 2".

2.1 Medium-range 3D Imaging Systems

Optical non-contact 3D imaging systems operating in the medium range, referred to here as ranging systems, typically use variations on laser time-of-flight to measure the distance to a point in the surface. The most common ranging systems can be broadly divided into those measuring the round-trip time t_L of the return signal and those measuring the phase shift φ_L of a modulated signal. Figure 2(a) illustrates the principle of time-of-flight (ToF) measurements based on measuring t_L of a pulse of light (pulse-based method). Figure 2(b) illustrates how the t_L can also be calculated by measuring φ_L of an amplitude-modulated (AM) laser beam (phase-based method). A limited number of commercial systems operate using frequency modulation[1] and more recent research is evaluating the use of chaotic modulation[2][3]. Figure 3 shows the range (referred to as depth) measurement uncertainty of phase-based and pulse-based systems in comparison to other common 3D imaging systems technologies.

Although there are many ways to perform pulse detection, the most common is the sample-and-hold method in which all incoming signals are sampled over a time interval but only the signal with the maximum amplitude is held. The sampling period is initiated by the emitted light pulse[4]. The time between the emitted pulse and the peak of the held signal is then used to calculate the round-trip time[5]. Other common pulse-detection methods include constant-fraction discrimination[5][6] and matched-filter detection[6]. Phase-shift detection is based on using a phase-locked loop to calculate the phase difference between to emitted and detected signal pulse[5].

For a pulse-based system, the distance to a point on the measured surface is calculated from the time t_L between the peak of the transmitted optical signal and the peak of detected return signal, as illustrated in Figure 2(a), such that
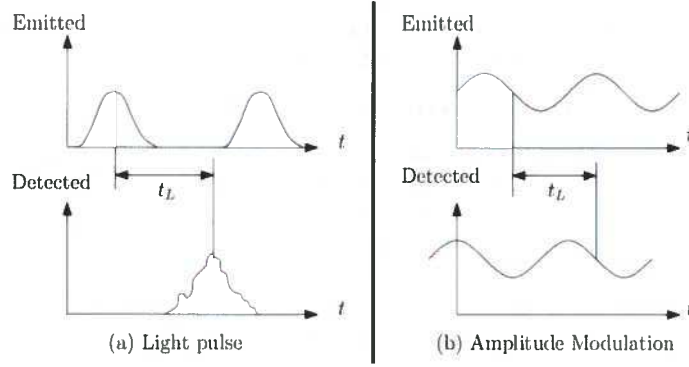
$$R = \frac{c\, t_L}{2} \tag{1}$$

Figure 2. Graphical illustration of round-trip time calculated using (a) the pulse-delay method and (b) the phase-shift method.

is the distance R from the origin of the system to a point on the surface and c is the speed of light in the conducting medium[5][7][8]. Note that (1) is a simplified form of the equation to illustrate the relationship so does not include factors such as index of refraction that can also affect the range value. The shape of the return pulse can be affected by factors such as include beam jitter, speckle noise, turbulence-induced scintillations, noise-equivalent power (NEP) from the detector and amplifier, system jitter, and density of photons arriving at the detector[6].
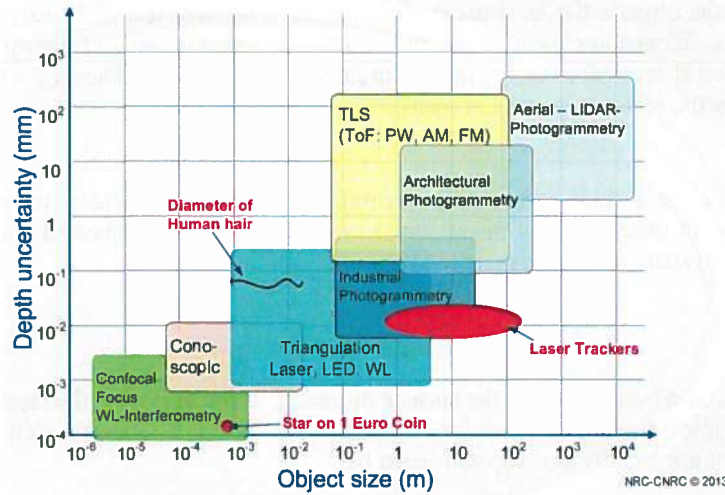
Figure 3. Expected depth (range) measurement uncertainty level as a function of depth-of-field/object size for different non-contact 3D imaging methods[9].

Equation (1) can be applied to phase-based systems, except that t_L is calculated using

$$t_L = \left(\frac{\varphi_L}{2\pi} + n\right) T \tag{2}$$

where φ_L is the phase difference between the emitted and detected signals, T is the period of the signal modulation, and n is the number of wavelengths included in the round-trip time[7]. Moreover, multiple wavelengths may be employed simultaneously to increase the depth resolution and to increase the size of the ambiguity interval (distance over which the range can be calculated without ambiguity)[7]. The smallest measurement uncertainties are observed for systems with short modulation periods (as will be explained in the next section); however, the size of the ambiguity interval is proportional to the modulation period so using multiple wavelengths provides a way to extend the ambiguity interval

while minimizing range measurement uncertainty[5]. In these systems, range measurement uncertainty predominantly arises from the length of the shortest wavelength used[7] and the uncertainty in the phase measurement system[5].

2.2 Factors Affecting Range Measurement Uncertainty

Factors affecting range measurement uncertainty can be broadly divided into internal factors and external factors. Internal factors are not under the control of the IUT operator so are not discussed in this article; rather, they are treated as a single factor affecting range measurement uncertainty and are assumed to have been quantified by the IUT manufacturer.

2.2.1 General Equations

In general, the range measurement uncertainty for pulse-based IUTs using rising-edge detection is

$$\sigma_{R_{pulse}} \sim \frac{c\, t_{rise}\sqrt{B_{pulse}}}{2\, P_{peak}} \tag{3}$$

where t_{rise} is the time required to complete the rising edge of the pulse. For phase-based IUTs, the range measurement uncertainty is

$$\sigma_{R_{AM}} \sim \frac{\lambda_{short}\sqrt{B_{AM}}}{4\,\pi\, P_{average}} \tag{4}$$

where, in the case of multi-frequency systems, λ_{short} is the shortest wavelength used by the IUT[8]. As was mentioned in Section 2.1, short wavelengths provide the least uncertainty but have the smallest ambiguity intervals, so phase-based IUTs typically use multiple frequencies to increase the ambiguity interval without sacrificing range measurement uncertainty. In these equations B represents the input measurement rate, (i.e. signal bandwidth) in units of hertz and P is the optical power detected by the receiver in units of watts[7][8].

2.2.2 External Factors

The primary external factors are surface effects and environmental effects. Consider, for example, the factors that contributed to the measurement uncertainty of phase-based systems. It has been reported that the range measurement uncertainty of a phase-based system can be approximated by

$$\sigma_{R_{AM}} \sim \frac{R_a\, R}{\sqrt{2\,\pi\, k\, \rho\, \cos(\alpha)}} \tag{5}$$

where α is the angle between the beam axis and the surface normal, ρ is the surface reflectance factor, $R_a = 1/(2\, T)$ is the length of the ambiguity interval, and k is a scalar multiplier[10]. This was a simplification of the an earlier study in which the range measurement uncertainty was approximated by

$$\sigma_{R_{AM}} \sim \frac{c\, T_{short}}{m} \sqrt{\frac{c\, h\, R^2}{8\,\pi\, f\, \eta\, \lambda\, A_R\, \bar{F}_T\, T_{int}\, \rho\, \cos(\alpha)}} \tag{6}$$

where $0 \leq m \leq 1$ is the modulation factor of the phase-based system, h is the Planck's constant, f is the fraction of the radiant flux reflected from the surface that arrives at the detector, η is the quantum efficiency of the photodetector, λ is the wavelength of the laser being modulated, A_R is the area of the receiver, $\bar{F}_T$ is the average radiant flux arriving at the surface, T_{int} is the time interval over which the signal is received, and ρ is the diffuse reflectance factor of the surface[11].

Of these factors, α, $\bar{F}_T$, and ρ are external so cannot be bundled into a vendor-supplied measurement uncertainty. Of particular interested is that increasing α increases range uncertainty, whereas selecting surfaces with higher ρ decreases uncertainty. It has been observed that the dynamic range of $\rho \cos \alpha / R^2$ of a phase-based system with $1 \leq R \leq 5$ metres can be less than 90 dB, although the dynamic range could practically exceed 100 dB due to the significant increase in specular reflection when α is approaches 0[11]. Meanwhile, $\bar{F}_T$ is primarily a function of the transmitted signal power[11] but is affected by the transmission medium so is somewhat unpredictable except under highly controlled conditions[12]. Signal attenuation of systems using infrared wavelengths can be affected by the presence of water vapor, carbon dioxide (for airborne systems), and suspended particulate matter[5][8]. Bright sunlight was also identified as a factor affecting the

ability to distinguish the optical signal from background optical noise[8], which is handled by employing an optical notch filter, albeit at the cost of further attenuating the incoming signal[5].

Even under ideal atmospheric conditions with ideal surfaces, temperature and pressure can have an effect of the emitted signal. The uncertainty associated with the index of refraction in air can be approximated by

$$u_{IR} \sim L_m \sqrt{\frac{c_P^2(\Delta P)^2 + c_T^2(\Delta T)^2}{3}} \tag{7}$$

where c_P^2 and c_T^2 are the frequency-specific sensitivity coefficients for pressure and thermal effects along the beam path. For example, the sensitivity coefficients for a laser with wavelength $\lambda=633$ nm propagating in dry air, the sensitivity coefficients are $c_P^2 = 2.7 \times 10^{-9}$ Pa^{-1} for pressure and $c_T^2 = -1.0 \times 10^{-6}$ $°C^{-1}$ for temperature[13]. Temperature and pressure variations along the optical path are not expected to significantly affect the round-trip time measured by ranging systems[14] but effects such as beam divergence and asymmetries in beam shape (divergence from assumed TEM00) can affect the shape of the return pulse in pulse-based systems[6]. Thermal gradients can also have an effect of the index of refraction so can also increase the uncertainty in the final range measurement.

Atmospheric turbulence can also result in beam spreading which results in the laser spot covering a larger portion of the surface than predicted for the ideal case[15]. Water droplets larger than the wavelength of the laser can result in beam broadening for linearly-polarized Gaussian beams used in lidar (light detection and ranging) systems, although the shape of the beam core, beam polarization and beam coherence all appeared unaffected[16].

In addition to environmental factors, characteristics of the beams themselves can introduce errors into the range measurement. Salo et al. discovered periodic relative range measurement errors were present in amplitude-modulated ranging systems, and that these errors could be correlated with the ranging system's modulation frequencies or their harmonics. They further showed that these errors could be corrected using Fourier analysis, although this is complicated by the fact that many manufacturers do not allow external access to the subsystems used to control the beam amplitude or to measure beam phase[34].

2.2.3 Surface-related External Factors

Surface effects include factors such as surface material properties, surface material geometry, and surface material state. Opacity of surface material is an important factor that affects both range measurement uncertainty and range measurement bias. Studies on a variety of marble surfaces as an example of partially-opaque surface material revealed that surface penetration introduced a range bias into measurement results obtained by ToF systems[17][18][19]. Figure 4 shows a demonstration of this effect by placing an opaque sheet of paper flat against a marble surface. Range measurements indicated a bias of approximately 5 mm where without surface penetration the range difference would have been approximately 0.1 mm. With regard to selection of a reference material for the assessment of range measurement error, care must be taken in selecting completely opaque surface materials to minimize the effect of the surface material on the observed range measurement error.

Even when a surface has been selected to be completely opaque, surface quality can affect range measurement results. One study showed that the presence of water on the surface can introduce a range measurement bias, although it was not been observed to affect range measurement uncertainty in that study[20]. Another study found that range measurement uncertainty was strongly affected by surface reflectivity, with the effect increasing with range[21]. Finally, material settling from the atmosphere, such as dust and snow, can further affect surface measurements.

2.2.4 Surface Orientation

Two surface types that are typically selected as reference surfaces are planar surfaces and spherical surfaces. Assuming a planar surface has been selected as reference surface; studies have shown that surface orientation can affect measurement uncertainty. A recent study of four ranging systems observed that as the surface orientation of an ideal planar surface was increased, resulting in an increased angle of incidence and an elongated beam footprint, measurement uncertainty increased[22]. Even when many of these errors are controlled in simulations, range uncertainty is still affected by factors such as slant angle such that measurement uncertainty, represented by SNR, increased with an increase in planar surface angle[6]. Similar experiments at NRC in 2010 confirmed this observation, observing an increase in range measurement uncertainty with surface orientation[23].
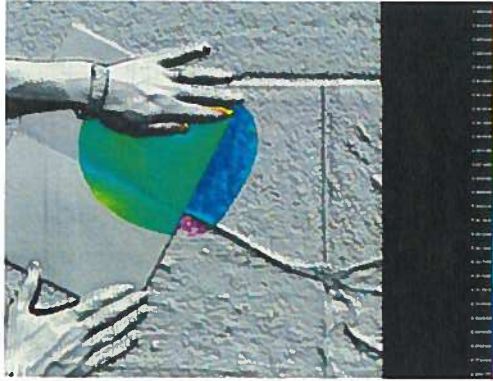
Figure 4. A demonstration of range measurement bias resulting from optical penetration of a marble surface. A 0.1 mm thick piece of paper represents an opaque surface held flat to the semi-opaque marble surface but penetration makes the marble surface appear offset by almost 5 mm from the paper[17].

3. RELATIVE RANGE ERROR ASSESSMENT

A relative range error assessment is an example of an artifact-mediated assessment, which provides a convenient way to evaluate the range error performance of an IUT. An artifact-mediated assessment is any assessment in which the performance of the IUT is compared against the performance of the selected RI using a well-characterized artifact as a mediating agent.

In this section we provide some background regarding the development of a range error protocol with focus on the choices of measurand, test protocol, and artifact selection. We then present the single-plane relative range error assessment method, followed by a detailed description of three-plane relative range assessment method. Results of a formal comparison of the single-plane and three-plane methods are described in Section 4.

3.1 ASTM E57.02 Relative Range Error Protocol

In 2006, the ASTM E57 committee was formed to develop standards to evaluate 3D imaging systems[24][25]. The E57.02 subcommittee on test methods initially began evaluating range error of medium-range 3D imaging systems based on distance, target reflectivity, angle of incidence, and azimuth (lateral rotation) angle using a combination of spherical and planar target structures[24][26]. A maximum range of 150 m for medium range systems was selected to represent the typical size of projects employing pulsed- and phase-based systems[26].

3.1.1 Artifact Selection

Based on early experiments[25][26][27][28], it was decided that a planar target would be used for range error analysis[24]. Spheres eliminated the need to orient the target but producing spheres 300 mm or more in diameter for testing the upper-end of the 150 m range was expected to be cost-prohibitive[26]. Moreover, planar surfaces were shown to generate less noise than spherical surfaces[29]. Planar surfaces are also reasonably easy for users to construct so the test would be accessible to a wide range of 3D imaging system users.

The use of real-world materials was also abandoned as being impractical given the large number of possible materials. SPECTRALON® (http://www.labsphere.com/), an industry-standard material for testing optical systems, was also considered but was discarded because of its cost and the fact that lasers operating in the wavelengths common to medium-range 3D imaging systems (500 nm to 1600 nm) penetrated the material by as much as 3 mm[24][30]. Further experimentation focused on surfaces made of aluminum that had been vapour blasted or sand blasted to provide a diffusely-reflecting surface[24]. In this paper, all target surfaces are planar aluminum surfaces that have been vapour-blasted to produce a diffusely-reflecting surface.

3.1.2 Relative versus Absolute Range Error

Ranging error has two primary components: a constant origin offset (R0) error and an incremental distance error[27]. Relative range error means that the distance being evaluated is the relative distance, or distance between two points, not

the absolute distance from the origin/center of the IUT to a point on a target. Because the origin of many 3D imaging systems is typically unknown or not readily measurable, using relative distance means that any test method to evaluate range error would not be restricted to certain classes of 3D imaging system. If the test method is further restricted such that the distance between the points is only along a line passing through the origin of the IUT and the points are located on the same side of the IUT, then the constant R0 error is effectively cancelled out so the distance error component of the ranging error dominates the resulting range error value.

3.2 Single-plane Relative Range Error

The setup for the single-plane relative range error test proposed by the ASTM E57 committee involves placing two target plates along the LOS as illustrated in Figure 5 such that the LOS passes through C_{near}, C_{far}, and O, and the normal vectors of the target-plate faces are aligned along the LOS with target plate face normal vectors directed toward O. The arrangement can also be generated using a single target plate moved to C_{near} and C_{far} as required. The RI (for example, a laser tracker) is used to assist in achieving this setup as closely as is practically achievable. In all cases the target plate is rigidly mounted so that it does not move during both RI and IUT measurement steps.
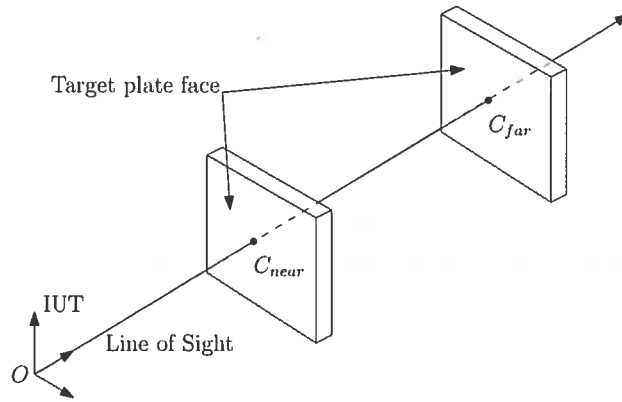

Figure 5. Near and far positions and orientations of the single-plane assembly.

3.2.1 Measuring the Reference Distance

A spherically-mounted retro-reflector (SMR) is used to obtain position measurements at widely-distributed points on the target-plate face so that a plane can be accurately fit to the measurement data obtained using the RI. Additional position measurements are obtained for all four sides bounding the target-plate face so that the bounds of the target-plate face can be established. Figure 6 shows the fit of all five planes. The target plate face is denoted S_{face} and the four sides are denoted S_{left}, S_{right}, S_{top} and S_{bottom}. The single-plane relative range error test proposed by the ASTM E57 committee does not specify how the five planes are fit; however, they would typically be obtained using either the least-median fit method described in the ASME Y14.5[31] or the Total Least-squares method[32].

Once the five planes have been generated, the single-plane relative range error test proposed by the ASTM E57 committee requires that these planes be used to estimate the reference geometric center of the target plate face. The proposed test does specify how this may be achieved. The geometric center can be defined as the theoretical center of mass, or centroid, of a representation of the target plate face using a structure of uniform density with bounds defined by the target plate edge. In this case, the geometric center would be the theoretical point on the uniform density structure that if placed on a balance point would result in the structure being in perfect balance. Because the geometric center is estimated from measurements of the five planes, it is referred to as a derived point to distinguish it from points obtained by direct measurement.

Practically, the geometric center of the target-plate face in the RI coordinate system is estimated from the intersection of S_{face}, the bisecting plane between S_{left} and S_{right}, and the bisecting plane between S_{top} and S_{bottom}. In the rare instance where either S_{left} and S_{right} or S_{top} and S_{bottom} are truly parallel, the bisecting plane is replace with a plane equidistant between the two planes. The geometric center of the target-plate face is estimated at C_{near} to obtain $g_{near} =$

$[x_{near} \quad y_{near} \quad z_{near}]^T$ and at C_{far} to obtain $\boldsymbol{g}_{far} = [x_{far} \quad y_{far} \quad z_{far}]^T$. The reference distance obtained from the RI is then found to be

$$d_{SinglePlane} = \left\| \boldsymbol{g}_{far} - \boldsymbol{g}_{near} \right\|_2 \tag{8}$$

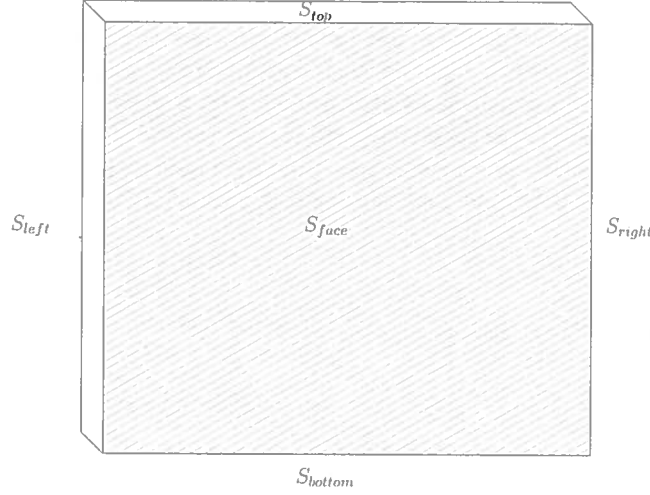where $\|x\|_2 = \sqrt{x \cdot x}$ is the Euclidean or L^2 norm.

Figure 6. Planes to be measured using an SMR and the RI.

3.2.2 IUT Distance Measurement

The IUT measurement of the distance between C_{near} and C_{far} requires estimating the position of the geometric centroid of the target plate face in the IUT reference frame. Centroid estimating is a two-stage process: fitting of a plane to the target plate face such that it is not affected by measurement results obtained from near the edges of the target plate face, and establishing the bounds on the plane such that they coincide with the edges of the target plate face. This requires that the measurement results obtained by the IUT include all four visible edges and that the edges are clearly distinguishable from the background such that all measurement results associated with the target plate face, including its edges, can be visually extracted from the scan data by the operator.
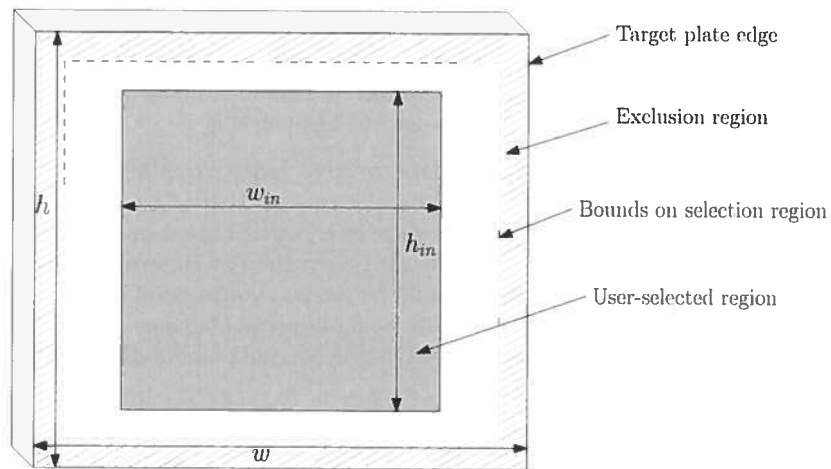

Figure 7. User-selected and Exclusion regions for the single-plane test method..

In the first stage, the operator visually selects a region on the target plate face that is sufficiently far from the edges that the resulting measurement set is unlikely to include edge-affected measurement results. In Figure 7, this region is indicated by the grey user-selected region. The region containing points that are likely to be affected by the edges is labeled the exclusion region in Figure 7 and denoted by diagonally-hashed shading. On the other hand, the selection region must be large enough that there are sufficient points in the region that the best-fit plane will be a good estimate of the target plate face. The maximum permissible size of the user-selected region is indicated in Figure 7 by a dashed line. A best-fit plane of infinite bounds is then fit to the measurement results in the user-selected region using the Total Least-squares method[32]. An example of the first stage of the single-plane method using data obtained from a square target plate can be seen in Fig 8(a).

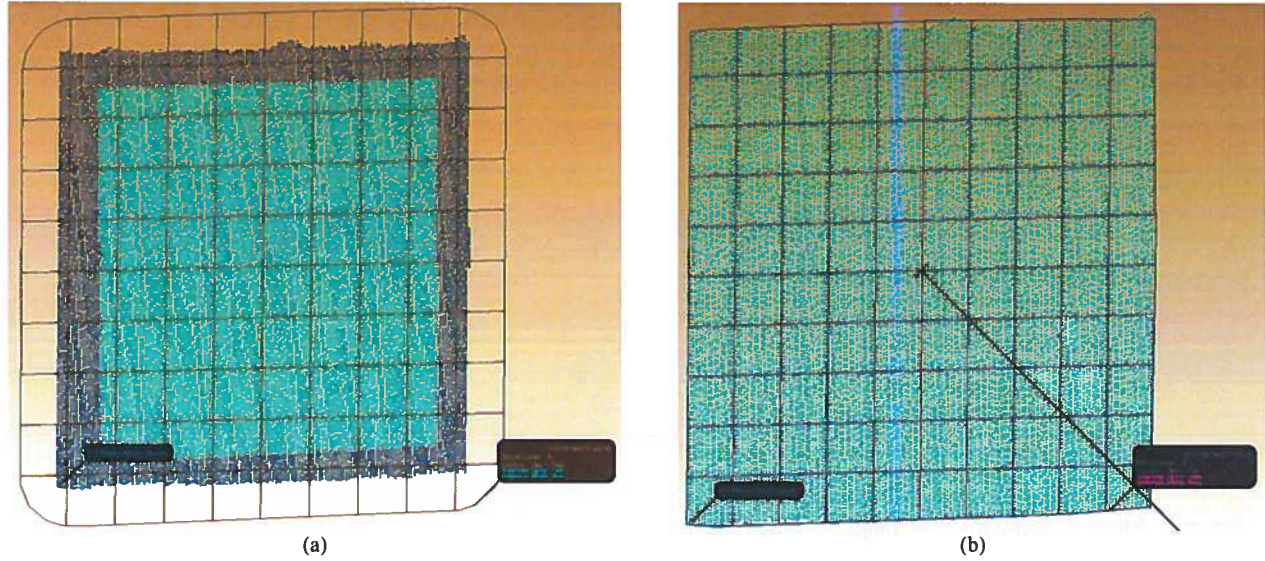(a)   (b)

Figure 8. Examples of Stage 1 and Stage 2 in the single-plane method for generating an estimate of the position of the geometric center of the target plate face. (a) Stage 1: Select a region (pale square region) and generate a total least-squares best-fit plane with infinite bounds (shown as a lined grid). (b) Stage 2: Bound the plane to encompass all IUT measurement results after removing measurements more than 2 standard deviations from the plane generated in Stage 1. The line points to the geometric center of the resulting bounded plane.

In the second stage, all measurement results more than 2 standard deviations of the plane-fit residuals from best-fit plane are removed from the scan of the target plate face. A bounding box is then constructed around the remaining measurement results and used to establish the bounds on the best-fit plane. Specifically, the target plate face edges are estimated to be the edges of the smallest rectangular bounding box that completely encloses all of the data. The geometric center of the bounded best-fit plane becomes the estimate of the geometric center of the target plate face. An example of the second stage of the single-plane method using data obtained from a square target plate can be seen in Figure 8(b).

The geometric center of the target-plate face is estimated at C_{near} to obtain $\hat{g}_{near} = [\hat{x}_{near} \quad \hat{y}_{near} \quad \hat{z}_{near}]^T$ and at C_{far} to obtain $\hat{g}_{far} = [\hat{x}_{far} \quad \hat{y}_{far} \quad \hat{z}_{far}]^T$. The reference distance is then found to be

$$\hat{d}_{SinglePlane} = \left\| \hat{g}_{far} - \hat{g}_{near} \right\|_2 \tag{9}$$

where the presence of the hat over the variables indicates that this is the estimate of the measurand obtained from the IUT.

3.2.3 Calculating Relative Range Error

The relative range error

$$E_{SinglePlane} = \hat{d}_{SinglePlane} - d_{SinglePlane} \tag{10}$$

is calculated to be the signed difference between the IUT and RI-generated distances between the geometric centres of the same target plate faces. Ideally the geometric centers should be close to the LOS as illustrated in Figure 5. Keeping the geometric centers close to the LOS minimizes the effect of cosine error on the relative range error, as illustrated in Figure 9. Cosine error is caused by a rotation, horizontal or vertical or both, of the line between the geometric centers from the LOS. This deviation allows angular encoder errors from the IUT and RI to be coupled to the relative range error. As can be seen in Figure 9, if one of the target planes is laterally offset from the other (represented by the position of C_{offset}), then a component of the distance d_{offset} is contributed by the lateral offset. The error associated with d_{offset} therefore includes error from the angular encoders. By contrast, the error associated with d_{min} comes entirely from the range measurement.
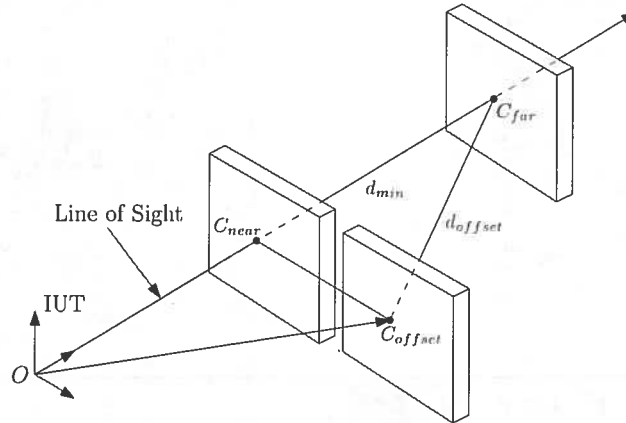

Figure 9. Effect of lateral offset on range measurement.

3.3 Three-plane Relative Range Error

A concern regarding the single-plane method is that it depends on how well the measured data is able to reproduce the edges of the target plate face. Figure 10 illustrates the problem for the situation in which there are multiple returns from the same optical signal. If the beam only illuminates the near surface (grey region to the right) then only a single return signal is generated. At the bottom of the image is a representation of the measured surface assuming no measurement noise for ease of illustration. As the beam passes the edge, multiple return signals are generated. How the edge is represented can vary from system to system depending on how they handle the multiple-return problem. In this illustration simple averaging is used, but other approaches, such as first-return and selection based on return intensity could also be employed.

Moreover, the system can only detect that a return signal exists, not from which portion of the beam it was generated, so all return signals are assumed to be from along the beam axis, even if the return signal was generated by a surface that is only illuminated by a portion of the surface not coinciding with the beam axis. In Figure 10, this would be represented by the top row of squares at the bottom of the figure. The result is an extension of the edge beyond the "true" edge, but by an amount that is determined by the minimum cut-off level of return signal intensity required to be identified as a valid return signal. Again, this varies among systems, particularly because some systems may apply internal data filtering as part of generating measurement results.

An alternative approach is to use a method that avoids using the edge-affected measurement results. The three-plane method, like the single-plane method, involves a first stage of selecting measurement results from within each of the three target plate faces that are not affected by the edges of the target plate faces. For each plate, a plane with infinite bounds is then generated. The difference is in the second stage: the geometric center is replaced with the derived POI of the three planes. From basic geometry, the intersection of two non-parallel planes generates a line, and the intersection of that line with a third plane that is not parallel to either of the other two generates a unique point. The distance between the three-plane assemblies is then calculated to be the distance between the POIs at C_{near} and C_{far}.
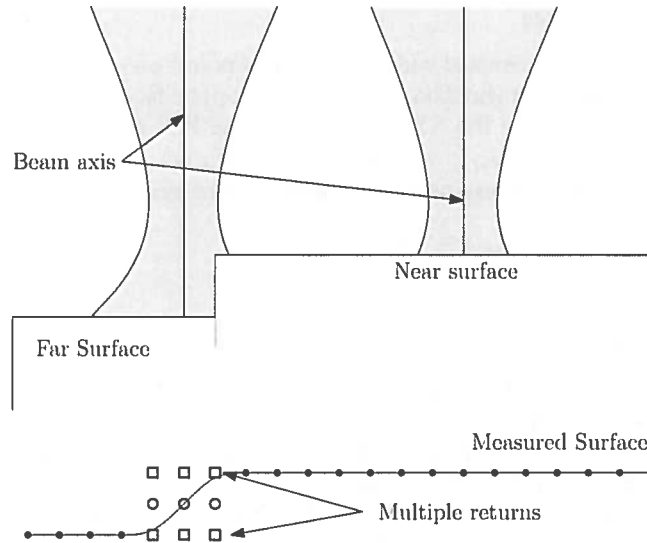
Figure 10. Illustration of edge location ambiguity. On the Measured Surface at the bottom of the figure, solid black circles indicate unambiguous measurement results, open squares indicate return signals, and the open circles indicate the average of the return signals associated with each measurement.

The trade-off for avoiding use of edge-affected measurement results is that the normal vectors of the planes are not oriented along the LOS so the beam footprint is elongated. As noted in Section 2.2.4, range measurement uncertainty increases with surface orientation. Figure 11 shows the result of a simulated optical pulse reflected from a planar surface with normal oriented at 60 degrees to the LOS. We see that the pulse is elongated in time, which can increase the uncertainty in calculating the round-trip time of the pulse, albeit primarily for surfaces with normal vectors oriented at large angles from the LOS. In practice, the orientation of the planes would be no more than 30 degrees to the LOS to reduce the effect of surface orientation on the uncertainty associated with the relative range error calculation.
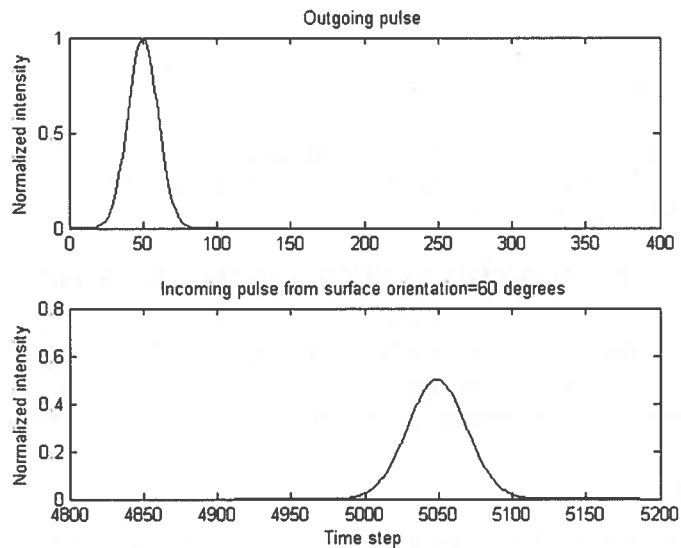

Figure 11. Simulated pulse reflected from a planar surface with normal oriented 60 degrees to the LOS. The top image shows the outgoing (emitted) pulse and the bottom graph shows the incoming (detected) pulse.

3.3.1 Measuring the Reference Distance

The RI is used to obtain position measurements at widely-distributed points on each of the three target-plate faces so that a plane can be accurately fit to the measurement data from each target plate face. The plane fit of each of the three planes are obtained using the method described in the ASME Y14.5[31]. The POI of the three-plane assembly is obtained at C_{near} to obtain $p_{near} = [x_{near} \quad y_{near} \quad z_{near}]^T$ and at C_{far} to obtain position value $p_{far} = [x_{far} \quad y_{far} \quad z_{far}]^T$ by calculating the POI of the three planes in the assembly. The reference distance for the RI is then found to be

$$d_{ThreePlane} = \left\| p_{far} - p_{near} \right\|_2.$$ (11)

3.3.2 IUT Distance Measurement

As with the RI distance measurement, the IUT distance measurement for the three-plane method differs from the single-plane method primarily in the second stage. In the first stage, the operator visually selects a region on each of the three target plate faces that is sufficiently far from the edges that the resulting measurement set is unlikely to include edge-affected measurement results. A best-fit plane of infinite bounds is then fit to the measurement results in the user-selected region for each of the three target plate faces using the Total Least-squares method[32]. In the second stage, the POI of the three planes is computed from the intersection of the three planes. The POI of the three-plane assembly is then obtained at C_{near} to obtain $\hat{p}_{near} = [\hat{x}_{near} \quad \hat{y}_{near} \quad \hat{z}_{near}]^T$ and at C_{far} to obtain position value $\hat{p}_{far} = [\hat{x}_{far} \quad \hat{y}_{far} \quad \hat{z}_{far}]^T$. Finally, the reference distance is then found to be

$$\hat{d}_{ThreePlane} = \left\| \hat{p}_{far} - \hat{p}_{near} \right\|_2$$ (12)

where the presence of the hat over the variables indicates that this is the estimate of the measurand obtained from the IUT.

Figure 12 shows how the distance between two three-plane assemblies can be performed using a commercial software package (in this case, IMInspect™ from InnovMetric Software Inc™). The measurement results for the three-plane assemblies at C_{near} and C_{far} is shown in grey, the best-fit planes are shown in blue and green for C_{near} and C_{far} respectively, and the line is used to calculate the distance between the POIs.

3.3.3 Calculating Relative Range Error

The relative range error

$$E_{ThreePlane} = \hat{d}_{ThreePlane} - d_{ThreePlane}$$ (13)

is calculated to be the signed difference between the IUT and RI-generated distances between the POIs of the same three-plane assemblies. As with the single-plane method, the POIs should ideally be close to the LOS so that the relative range error is minimally affected by cosine errors.

4.   RESULTS OF METHOD COMPARISON TEST

Experiments were conducted at the 3-Dimensional (3D) metrology laboratory at the NRC (NRC-3DM) to compare the ease-of-use and performance of the single-plane and three-plane methods. The three-plane method was developed at NRC to address concerns about the single-plane method's dependence on locating the target plate face edges in IUT measurement results. The effects of surface orientation are more easily quantified so can be factored into any possible traceability assessments.

4.1 Target Plate Assemblies

Single-plane and three-plane assemblies were constructed at the NRC-3DM laboratory to be mounted on a 2.5 m rail system. A laser tracker was used as the RI for these experiments. Two medium-range ToF laser-based ranging systems were employed as examples of two scanning technologies: pulse-based systems and phase-based systems. Because comparison of these technologies is not the focus of the experiment, the system manufacturer and underlying scanning technology is not indicated here to avoid implication of which technology might produce "better" results. The two systems are simply referred to as IUT-Phase (Phase-based IUT) and IUT-Pulse (Pulse-based IUT).
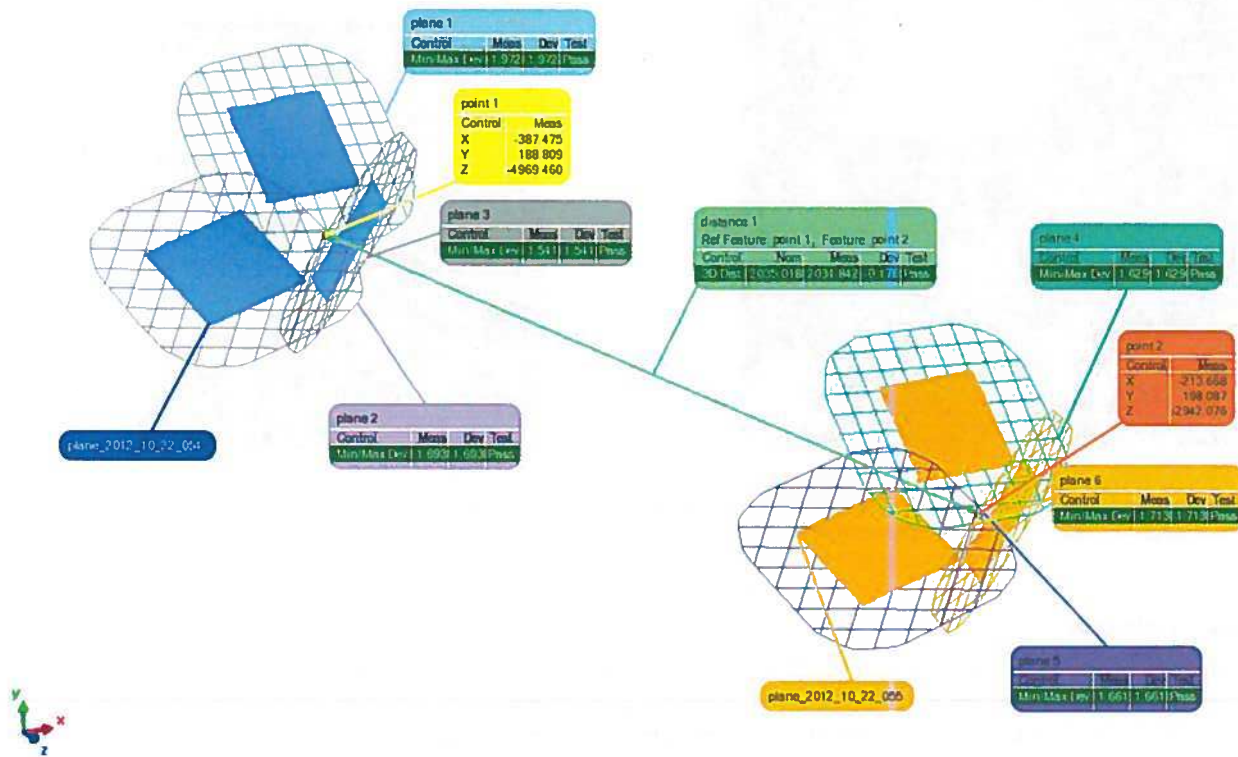
Figure 12. Calculation of distance between POIs of near and far three-plane assemblies at C_{near} and C_{far}.

Figure 13 shows the target plate assemblies used at the NRC-3DM laboratory. Figure 13(a) shows the three-plane assembly developed, consisting of three target plates attached to common mounting plate. The target plates are oriented at approximately 30 degrees to the LOS to minimize the effect of surface orientation on measurement uncertainty while ensuring that the planes are not mutually parallel. Figure 13(b) shows a single-plane assembly. Both single-plane and three-plane assembly target face plates are constructed from aluminum and were vapour-blasted to ensure a diffusely-reflecting surface.

4.2 Modeling the Target Plate Assemblies

A method was developed at NRC to simplify the processes of obtaining the reference distances. This involves virtually linking a digital model of the target plate assembly to the positions of SMR mounts on the mounting plate. The RI is used to obtain measurement results as described in Section 3.2.1 and Section 3.3.1 to create a virtual model of the single-plane or three-plane assembly. Specifically, the assembly is placed in a position near the RI (to minimize RI measurement uncertainty), then a 1.5 inch (38.1 mm) diameter SMR is used to perform three to five measurements of each of the four sides of each of the target plates and at least five measurements of the front of each of the target plates. For each of planar surfaces, measurements are performed at positions far from each other to ensure that the final model is a reasonable representation of each planar surface.

All RI measurement results are combined into a digital model so that as the target plate assembly is moved the reference geometric center or POI can be obtained by simply re-probing SMR mounts on the mounting plate. This avoids the time and potential for operator error inherent in re-measuring the target plates using the RI. Figure 12 illustrates the side and front view of this arrangement using the single-plane assembly as an example. The SMR mounts can be seen in the images of the target plate assemblies in Figure 13.
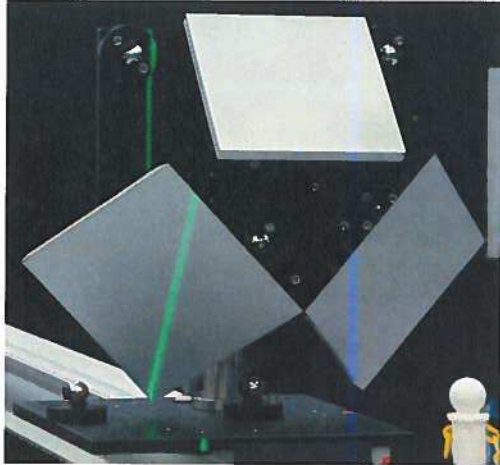
Figure 12. Target plate assemblies used at the 3-Dimensional Metrology Laboratory at NRC. (a) Three-plane assembly developed by NRC. (b) Single-plane assembly.

4.3 Data Collection

The target plate assembly is placed in the near and far position on the rail, separate by approximately 2 metres. At each position, both the SMR positions and a scan of the target-plate surface are obtained. For each IUT and target plate assembly, a single RI and IUT measurement set is performed to generate a single reference and IUT distance value. The relative range error for each RI-IUT pair for each IUT and each target plate assembly was then calculated using (10) and (13) as appropriate. The process was repeated 6 times to determine the dispersion in relative range error results.
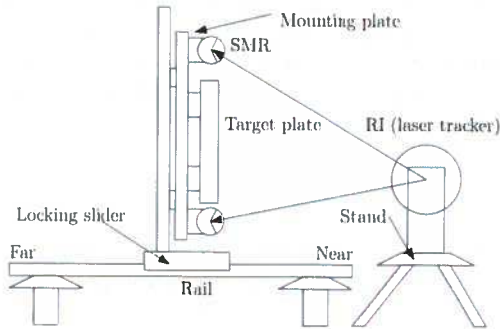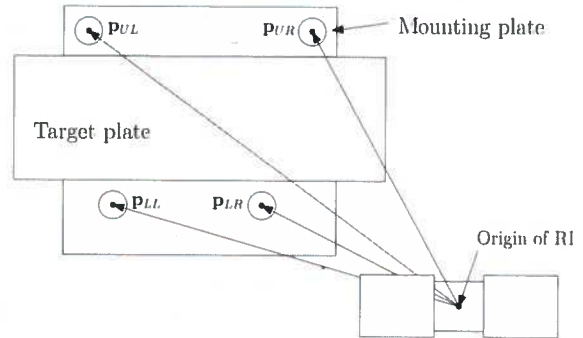
Figure 13. Test setup using a rail-mounted target plate for the single-plane assembly. (a) Side view showing the position of the RI, target plate, and SMRs. (b) Front view showing the position of the RI, in front and to one side of the target plate, as well as the distribution of the SMRs.

For each IUT, the standard deviations of the plane-fit residuals were recorded for the C_{near} position. This position was chosen as most likely to provide the smallest measures of residual dispersion for each IUT. The first stage plane fit was performed without filtering or outlier removal.

4.4 Effect of User Selection

The effect of the region selected by the user on the best-fit plane was examined by performing a series of 10 selections of the user-selected region by the same user. The size and shape of the user-selected regions were varied within the limitations that the selected points must be within the bounds on the user-selected region as indicated in Figure 7 and

must have a minimum dimension of 100 by 100 data points. The variation in best-fit residuals and plane equation parameters were then examined.

As can be seen in Table 1, plane construction for the single-plane method was highly consistent. The A, B, and C parameters of the plane varied by an amount below the resolution of the test, and, the standard deviation (St. Dev.) of the D parameter was only 0.0196 mm. The residuals of the best-fit plane were also highly consistent, varying by only 0.0021 mm. Although user-selection clearly has an effect on the resulting best-fit plane, the effect is in the order of fractions of a millimeter, well below the expected measurement uncertainty of a typical medium-range system. Given the selection process is also used for the three-plane method, it can be concluded that the user-selection process is not a significant issue for either method.

Table 1. Standard equation of A plane ($Ax + By + Cz = D$) for the single-plane method. The last column represents the standard deviation of the absolute values of the dispersion of the Plane-Fit residuals.

Repetition	A (mm)	B (mm)	C (mm)	D (mm)	σ (mm)
1	0.0662	0.0031	0.9978	5192.465	0.167
2	0.0662	0.0031	0.9978	5192.459	0.167
3	0.0661	0.0030	0.9978	5192.481	0.169
4	0.0663	0.0031	0.9978	5192.448	0.164
5	0.0661	0.0030	0.9978	5192.472	0.168
6	0.0662	0.0030	0.9978	5192.470	0.167
7	0.0662	0.0031	0.9978	5192.467	0.165
8	0.0658	0.0030	0.9978	5192.516	0.162
9	0.0663	0.0031	0.9978	5192.448	0.167
10	0.0661	0.0030	0.9978	5192.480	0.165
Mean	**0.0661**	**0.0030**	**0.9978**	**5192.471**	**0.166**
St.Dev.	**0.0001**	**~0**	**~0**	**0.0196**	**0.0021**

4.5 Dispersion of Best-fit Residuals

The dispersions of the plane fit residuals were obtained for stage 1 of the single-plane and three-plane methods. Table 2 shows the dispersions represented by the standard deviation of the absolute values of the residuals. The dispersions were compared within each IUT to using a t-test to determine whether there was a significant difference between methods for each IUT.

Table 2. Dispersion of Best-Fit Residuals at C_{near}

IUT	Repetition	Standard deviation of the absolute value of the residual dispersion (mm)			
		Single-plane	Three-plane		
IUT-Phase	1	0.167	0.192	0.198	0.200
	2	0.150	0.212	0.179	0.195
	3	0.164	0.172	0.179	0.173
	4	0.157	0.221	0.205	0.184
	5	0.186	0.259	0.260	0.188
	6	0.163	0.182	0.177	0.174
	Mean	**0.165**	**0.197**		
	St. Dev.	**0.012**	**0.027**		
IUT-Pulse	1	1.468	1.180	1.188	1.183
	2	1.417	1.091	1.116	1.107
	3	1.462	0.944	0.958	0.960
	4	1.185	0.928	0.951	0.947
	5	1.454	1.038	1.058	1.063
	6	1.252	1.037	1.051	1.054
	Mean	**1.373**	**1.047**		
	St. Dev.	**0.123**	**0.086**		

For IUT-Phase the probability of a significant difference between the single-plane and three-plane methods is $p = 0.009$, which is less than the $p = 0.05$ probability required to declare the difference significant, meaning a probability

less than $p = 0.05$ is required to declare a significant difference. As a result, we conclude that there is a statistically significant difference in residual dispersions between methods. From Table 2 the dispersions for IUT-Phase were 0.165 ± 0.012 mm for the single-plane method and 0.197 ± 0.027 mm for the three-plane method so the dispersions for the three-plane method were significantly larger than for the single-plane method. This is expected because the planes in the three-plane method have normal oriented at 30 degrees to the LOS so should have a greater dispersion. IUT-Phase is a phase-based system so the beam is moving during acquisition. This results in a "smearing" of the return signal over the angled surface, effectively blurring the measurements from three-plane surfaces slightly. As a result, measurement uncertainty, hence plane-fit residuals, will be significantly higher for the three-plane method than for the single-plane method. Practically, the difference is in the order of tens of micrometers so the contribution to total measurement uncertainty is small; one order of magnitude less than the observed standard deviation of the residual dispersion.

For IUT-Pulse the probability of a significant difference between the single-plane and three-plane methods is $p \approx 0$, which is less than the $p = 0.05$ probability required to declare the difference significant. As a result, we conclude that there is a statistically significant difference in residual dispersions between methods. From Table 2 the dispersions for IUT-Pulse were 1.373 ± 0.123 mm for the single-plane method and 1.047 ± 0.086 mm for the three-plane method.

4.6 Relative Range Error

The relative range errors were calculated for the single-plane and three-plane methods. Tables 3 and 4 show the relative range error values for IUT-Phase and IUT-Pulse respectively. The relative range errors were compared within each IUT to using a t-test to determine whether there was a significant difference between the methods for each IUT. Unlike the IUT-Phase, the IUT-Pulse is minimally affected by beam motion so unless the surface is highly oriented with respect to the LOS, the change in measurement uncertainty should be small. As discussed in Section 3.3.2, increased surface orientation can result in spreading of the return pulse; however if the pulse shape is sufficiently close to a square pulse that the transitions are relatively steep then a 30 degree surface orientation should have minimal effect on the final measurement.

Table 3. Relative Range Error IUT-Phase

Method	Repetition	$\hat{d}$ (mm) (IUT)	d (mm) (RI)	E (mm)
Single-plane	1	2034.727	2035.002	-0.275
	2	2033.099	2033.368	-0.269
	3	2030.652	2030.891	-0.239
	4	2034.768	2035.047	-0.279
	5	2034.656	2034.895	-0.239
	6	2034.614	2034.907	-0.293
		Mean Absolute (mm)		0.266
		St. Dev. Absolute (mm)		0.022
Three-plane	1	2034.842	2035.018	-0.176
	2	2034.661	2035.005	-0.344
	3	2032.753	2032.843	-0.090
	4	2032.715	2032.880	0.165
	5	2034.868	2035.059	0.191
	6	2034.858	2035.048	0.190
		Mean Absolute (mm)		0.193
		St. Dev. Absolute (mm)		0.083

For IUT-Phase the probability of a significant difference in relative range error between the single-plane and three-plane methods is $p = 0.064$, which is greater than the $p = 0.05$ probability required to declare the difference significant. We conclude that there is no significant difference in relative range errors between methods. From Table 3 the relative range errors for IUT-Phase were 0.266 ± 0.022 mm for the single-plane method and 0.193 ± 0.083 mm for the three-plane method.

For IUT-Pulse the probability of a significant difference in relative range error between the single-plane and three-plane methods is $p = 0.724$, which is greater than the $p = 0.05$ probability required to declare the difference significant. We conclude that there is no significant difference in relative range errors between methods. From Table 4 the relative range

errors for IUT-Pulse were 0.173 ± 0.128 mm for the single-plane method and 0.144 ± 0.152 mm for the three-plane method.

Table 4. Relative Range Error IUT-Pulse

Method	Repetition	$\hat{d}$ (mm) (IUT)	d (mm) (RI)	E (mm)
Single-plane	1	2034.953	2035.002	-0.049
	2	2033.344	2033.368	-0.024
	3	2031.250	2030.891	0.359
	4	2035.315	2035.047	0.268
	5	2035.049	2034.895	0.154
	6	2035.092	2034.907	0.185
	Mean Absolute (mm)			**0.173**
	St. Dev. (mm)			**0.128**
Three-plane	1	2035.44	2035.018	0.426
	2	2034.994	2035.005	-0.011
	3	2032.731	2032.843	-0.112
	4	2032.844	2032.880	-0.036
	5	2034.863	2035.059	-0.196
	6	2034.967	2035.048	-0.081
	Mean Absolute (mm)			**0.144**
	St. Dev. (mm)			**0.153**

4.7 Advantages and Disadvantages of Both Methods

The results presented in the preceding section indicate that the single-plane and three-plane methods are not significantly different with regard to generating a relative range error value. Choice of which method to use should, therefore, be based on other considerations. Here, we summarize the advantages and disadvantages of both methods.

For the single-plane method, one of the advantages is that the artifact is relatively simple to construct, consisting only of a single planar surface. The three-plane method requires a more complex structure that may not be feasible for some testing facilities to construct.

For the three-plane method, the primary advantage is that the method avoids tying the relative range error value to the location of the edges of the planar surface. Moreover, the process is amenable to automated edge region removal to minimize the effect of edge-affected measurement results on the relative range error method.

5. CONCLUSIONS

Despite the effect of surface orientation on residual dispersion in stage 1 of both methods, the resulting relative range error values generated by both methods are not significantly different. It can be concluded that strictly for purposes of measuring relative range error both methods produce equivalent results.

The three-plane method represents a trade-off in avoiding edge effects and at the cost of potentially increasing the residual dispersion in stage 1 of the method. It was observed, though, that the effect on residual dispersion may be IUT-dependent, given it was observed that for IUT-Pulse the three-plane method had a significantly lower residual dispersion, not higher as expected.

User selection of the plane-fit region in stage 1 of both methods was observed to introduce some uncertainty into both test methods but that the effect was well below the expected measurement uncertainty of the typical medium range systems currently on the market. It was concluded that the user-selection approach advocated in the proposed ASTM E57.02 relative range standard does not represent a significant issue.

ACKNOWLEDGEMENTS

REFERENCES

[1] Dupuy, D. and Lescure, M., "Improvement of the FMCW Laser Range-Finder by and APD Working as an Optoelectronic Mixer," IEEE Transactions on Instrumentation and Measurement 51(5), 1010-1014 (2002).

[2] Lin, F.-Y. and Liu, J.-M., "Ambiguity Functions of Laser-Based Chaotic Radar," IEEE Journal of Quantum Electronics 40(12), 1732-1738 (2004).

[3] Lin, F.-Y. and Liu, J.-M., "Chaotic Lidar," IEEE Journal of Selected Topics in Quantum Electronics 10(5), 991-997 (2004).

[4] Amann, M.-C., Bosch, T., Myllyä, R. and Rioux, M., "Laser ranging: a critical review of usual techniques for distance measurement," Optical Engineering 40(1), 10-19 (2001).

[5] Carmer, D.C. and Peterson, L.M., "Laser Radar in Robotics," Proceedings of the IEEE 84(2), 299-320 (1996).

[6] Grönwall, C., Steinvall, O., Gustafsson, F. and Chevalier, T., "Influence of Laser Radar Sensor Parameters on Range Measurement and Shape Fitting Uncertainties," Linköping University, Report LiTH-ISY-R-274 (2006).

[7] Wehr, A. and Lohr, U., "Airborne laser scanning–an introduction and overview," ISPRS Journal of Photogrammetry and Remote Sensing 54(2-3), 68–82 (1999).

[8] Baltsavias, E.P., "Airborne laser scanning: basic relations and formulas," ISPRS Journal of Photogrammetry and Remote Sensing 54(2-3), 199-214 (1999).

[9] Robson, S., Beraldin, J-A, Brownhill, A. and MacDonald, L., "Artefacts for optical surface measurement," Proceedings of the SPIE 8085: Videometrics, Range Imaging, and Applications XI, (2011).

[10] Hebert, M. and Krotkov, E., "3D measurements from imaging laser radars: how good are they?," Image and Vision Computing 10(3), 170–178 (1992).

[11] Nitzan, D., Brain, A.E. and Duda, R.O., "The Measurement and Use of Registered Reflectance and Range Data in Scene Analysis," Proceedings of the IEEE 65(2), 206-220 (1977).

[12] Estler, W.T., Edmundson, K.L., Peggs, G.N. and Parker, D.H., "Large-Scale Metrology–An Update," CIRP Annals–Manufacturing Technology 51(2), 587-609 (2002).

[13] ASME B89.4.19, [Performance Evaluation of Laser-Based Spherical Coordinate Measurement Systems], ASME (2006).

[14] Boehler, W., Vicent, M.B. and Marbs, A., "Investigating laser scanner accuracy," The International Archives of Photogrammetry, Remote Sensing and Spatial Information Sciences, vol. XXXIV (2003).

[15] Yura, H.T., "Atmospheric Turbulence Induced Laser Beam Spread," Applied Optics 10(12), 2771-2773 (1971).

[16] Ryan, J.S. and Carswell, A.I., "Laser beam broadening and depolarization in dense fogs," Journal of the Optical Society of America 68(7), 900-908 (1978).

[17] El-Hakim, S. F., Beraldin, J.-A., Picard, M. and Cournoyer, L., "Surface Reconstruction of Large Complex Structures from Mixed range Data–The Erechtheion Experience," Proceedings of the XXI Congress of the International Society for Photogrammetry and Remote Sensing 37(B5), (2008).

[18] Godin, G., Rioux, M., Beraldin, J.-A., Levoy, M., Cournoyer, L. and Blais, F., "An assessment of laser range measurement on marble surfaces," Proceedings of the 5th Conference on Optical 3D Measurement Techniques, (2001).

[19] Guidi, G., Remondino, F., Russo, M. and Spinetti, A., "Range sensors on marble surfaces: quantitative evaluation of artifacts," Proceedings of the SPIE 7447: Videometrics, Range Imaging, and Applications X, (2009).

[20] Lichti, D.D. and Harvey, B.R., "The effects of reflecting surface material properties on time-of-flight laser scanner measurements," Proceedings of the Symposium on Geospatial Theory, Processing and Applications. ISPRS Commission IV, (2002).

[21] Hancock, J., Langer, D., Hebert, M., Sullivan, R., Ingimarson, D., Hoffman, E., Mettenleiter, M. and Froehlich, C., "Active laser radar for high-performance measurements," Proceedings of the IEEE International Conference on Robotics and Automation vol. 2, 1465-1470 (1998).

[22] Mechekle, K., Kersten, T.P. and Lindsaedt, M., "Comparative investigations into the accuracy behavior of the new generation of terrestrial laser scanning systems," Optical 3-D Measurement Techniques VIII, Gruen/Kahmen (Eds.), vol. I, 319-327 (2007).

[23] Mak, N., Beraldin, J.-A., Cournoyer, L. and Picard, M., "A distance protocol for mid-range TLS in support of ASTM-E57 standards activity," International Archives of Photogrammetry, Remote Sensing and Spatial Information Sciences XXXVIII(5), (2010).

[24] Cheok, G.S., Lytle, A.M. and Saidi K.S., "ASTM E57 3D Imaging Systems Committee: An Update," Proceedings of the SPIE 6950: Laser Radar Technology and Applications XII, (2008).

[25] Beraldin, J.-A., Cournoyer, L., Picard, M. and Blais, F., "Proposed procedure for a distance protocol in support of ASTM-E57 standards activities on 3D imaging," Proceedings of the SPIE 7239: Three-dimensional Imaging Metrology, (2009).

[26] Cheok, G.S., Saidi, K.S. and Lytle, A.M., "Evaluating a Ranging Protocol for 3D Imaging Systems," Proceedings of the 24th International Symposium on Automation & Robotics in Construction, (2007).

[27] Bridges, R., "Ways to verify performance of 3D imaging instruments," Proceedings of the SPIE 7239: Three-dimensional Imaging Metrology, (2009).

[28] Cheok, G.S., Saidi, K.S., Franaszek, M., Filliben, J.J. and Scott, N.A., "Characterization of the Range Performance of a 3D Imaging System," NIST TN 1695, (2011).

[29] Beraldin, J.-A., "Basic Theory on Surface Measurement Uncertainty of 3D Imaging Systems," Proceedings of the SPIE 7239: Three-Dimensional Imaging Metrology, (2009).

[30] Cheok, G.S., Saidi, K.S. and Franaszek, M., "Target-Penetration of Laser-Based 3D Imaging Systems," Proceedings of the SPIE 7239: Three-dimensional Imaging Metrology, (2009).

[31] ASME Y14.5.1M, [Mathematical Definition of Dimensioning and Tolerancing Principles], ASME, (2004).

[32] Golub, G. H. and Van Loan, C.F., "An Analysis of the Total Least Squares Problem," SIAM Journal of Numerical Analysis 17(6), 883–893 (1980).

[33] ASTM E2544-11a, [Standard Terminology for Three-Dimensional (3D) Imaging Systems], ASTM International, (2011).

[34] Salo, P., Jokinen, O. and Kukko, A., "On the calibration of the distance measuring component of a terrestrial laser scanner," The International Archives of the Photogrammetry, Remote Sensing and Spatial Information Sciences XXXVII(B5), 1067-1071 (2008).